



The effects of thermal power and deposition time on the structural characteristics of ZnO nanorods and their optical properties for photovoltaic applications

S. Nasih¹ · A. Dlool¹ · G. El Hallani² · N. Fazouan¹ · E. H. Atmani¹ · A. Liba²

Received: 15 February 2020 / Accepted: 18 July 2020 / Published online: 7 August 2020
© Springer-Verlag GmbH Germany, part of Springer Nature 2020

Abstract

In this study, zinc oxide nanowires are elaborated by the hydrothermal method using a microwave furnace, which varies power and deposition times. The growth of nanowires is done on a buffer layer deposited on glass substrates using the sol–gel method associated with spin-coating. The X-Ray Diffraction (XRD) spectrums indicate that the obtained nanowires are well oriented in (002) plane according to the hexagonal wurtzite phase. The density and length of these nanowires increase while their diameter decreases with the deposition time and the microwave power. For high powers and longer deposition times, the ZnO nanowires adopt a pyramidal shape due to the low concentration of OH⁻ hydroxides in the deposition solution. The elaborated nanowires have an optical transmittance level in the visible region of about 90% with a red shift of the optical gap as the deposition time increases qualifying them for photovoltaic and other optoelectronic applications. A correlation between the diameter of the nanowires and their optical gap has been found which illustrates the narrow relationship between the structural, electronic, and optical aspects of these nanowires.

Keywords ZnO nanowires · Hydrothermal technique · Power furnace · Time deposition · Structural and optical correlation · Photovoltaic application

1 Introduction

In recent years, there was immense interest in semiconductor nanostructures due to their unique optoelectronic properties [1–5]. Among these nanostructures, ZnO is one of the most promising materials due to its direct bandwidth of 3.3 eV and high excitonic binding energy of 60 meV [6]. ZnO-based nanostructures have a wide range of applications; it can be used in light-emitting diodes (LEDs) [7], UV nanolasers [8], field-effect transistors [9], solar cell electrodes [10, 11] and nanogenerators [12]. In all these applications, one of the main objectives is to control the morphology, size, and

density of ZnO nanowires as these parameters have a major impact on the electronic and optical properties of ZnO.

Many deposition methods were used to develop ZnO nanowires, including vapor–liquid–solid (VLS) [13, 14], chemical vapor deposition (CVD) [15, 16] and metal–organic chemical vapor deposition (MOCVD) [17, 18]. Most of these deposition techniques are expensive and require special high-temperature treatment. However, the hydrothermal technique has the advantage of being less expensive since it is carried out in solution and operating at low temperatures [19]. Many reports on the hydrothermal method for nanowires growth have been published in the literature [20–26]. The major disadvantage of the hydrothermal method is the duration of the synthesis process. Indeed, the synthesis can take several hours to days. However, there are a few reports that used commercial microwaves as a furnace. Ayala Torres and al [27]. have developed nanowires using a commercial microwave at different powers between 350 and 700 W for growth time from 5, 20 and 35mins. Husnu et al. [28] also used the same processing method, from which they took three power values (120, 385, and 700 W) for growth time from 30, 10 and 3 min, respectively.

✉ N. Fazouan
fazouan@yahoo.fr

¹ Laboratory of Physics of Condensed Matters and Renewables Energies, Hassan II University, Faculty of Sciences and Technologies, B.P 146, 20650 Mohammedia, Morocco

² Laboratory of Materials Physics, Sultan Moulay Slimane University, Faculty of Sciences and Technologies, B.P 523, 23000 Beni Mellal, Morocco

Several parameters have significant effects on the morphology and aspect ratio of ZnO nanowires. Some of the main parameters involved in hydrothermal synthesis include precursor concentration, pH solution, growth time, growth temperature, and seed layer. The literature review showed that most studies on the growth of ZnO nanowires by hydrothermal method showed an increase in the average length and diameter of the nanowires as a function of temperature and deposition time [29–31].

Our work lies in the fact to synthesize well-oriented ZnO nanowires with good structural and optical properties using the principle of hydrothermal technique but at atmospheric pressure with a commercial microwave oven furnace of variable powers and at very short synthesis times. The ZnO nanowires are developed at different microwave powers (80, 120, and 400 watts) and different deposition times. Several techniques are used to characterize these nanowires, including X-ray diffraction (XRD) for structural study, scanning electron microscopy (SEM) for morphological study, and UV–Visible spectrophotometry for optical characterization.

2 Experimental method

2.1 ZnO seed layer

A buffer layer of ZnO was used to catalyze the ZnO nanowires growth. The seed layer was elaborated by the spin coating method by mixing zinc acetate dihydrate ($\text{Zn}(\text{CH}_3\text{COO})_2 \cdot 2\text{H}_2\text{O}$) (0.03 M) as a precursor, ethanol (50 ml) and monoethanolamine (MEA) as a solvent and a stabilizer, respectively. The mixture was well stirred for 1 h and spin-coated on glass substrates. The used glass substrates were cleaned with detergents, acetone, and ethanol, before being finally rinsed with distilled water and dried. We have used the same process as indicated in Fig. 1 to elaborate the ZnO seed layer [32].

2.2 ZnO nanowires growth

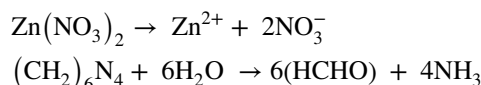
For the preparation of nanowires ZnO, an equimolar mixture of 0.05 M of zinc nitrate $\text{Zn}(\text{NO}_3)_2$ and hexamethylenetetramine HMTA dissolved in a volume of 50 ml of deionized water with a resistivity of $18\text{M}\Omega\text{cm}$ has been prepared. Once the solution was prepared, the seeded samples were immersed in it to maximize heating effects. The hydrothermal technique based on a microwave furnace of variable power was used to heat the deposition solution for the growth of ZnO nanowires at different powers and growth times.

The crystallographic phase of our samples was obtained using a Bruker D8 advance X-ray diffractometer operating at (40 kV, 40 mA) and equipped with a $\text{Cu}_{\text{K}\alpha 1}$ anti-cathode

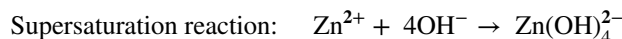
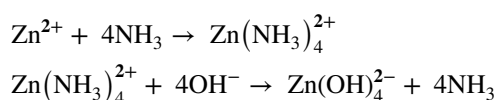
with wavelength $\lambda = 1.5406 \text{ \AA}$. We used field effect scanning electron microscopy (FESEM) to see the morphology of our samples. Finally, the optical measurements were made by the UV–Vis spectrophotometer via integrating sphere and double light beams of the "T92 + PG Instrument" type allowing to carry out measurements in reflectivity or transmittance modes depending on the arrangement of the sample in the integrating sphere. A correct transmittance (reflectance) measurement by an integrating sphere can be performed by placing the sample to be measured at one of its aperture. All measurement light is irradiated onto the photosensitive surface of the detector, placed at an aperture at the bottom of the integrating sphere, after being scattered inside it during both baseline correction and sample measurement.

The procedure for developing ZnO nanowires is shown in Fig. 1. During the decomposition of zinc nitrate $\text{Zn}(\text{NO}_3)_2$ and hexamethylenetetramine HMTA in deionized water at high temperature, the concentration of Zn^{2+} and OH^- increases accordingly. When the concentration of Zn^{2+} , OH^- and $\text{Zn}(\text{OH})_4^{2-}$ reaches a supersaturated degree, it leads to the rapid nucleation of ZnO and the formation of ZnO nanowires in the reactive solution with a suitable temperature. The aqueous solutions of zinc nitrate and HMTA can produce the following chemical reactions [33]:

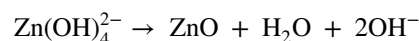
Decomposition reactions:



Zincate formation reactions:



ZnO nanowire growth reaction:



The growth of ZnO nanowires is controlled by the supersaturation of the reactants. Indeed, high levels of supersaturation, facilitate nucleation and low levels of supersaturation contribute to the growth of the ZnO crystal [34]. If a lot of hydroxide OH^- ions are produced in a short time, the Zn^{2+} ions will precipitate quickly due to the high pH (basic environment) and therefore, they would contribute little to the growth of ZnO nanowires and instead favorize the growth of nanoflowers as reported by Shin et al. [35]. Thus,

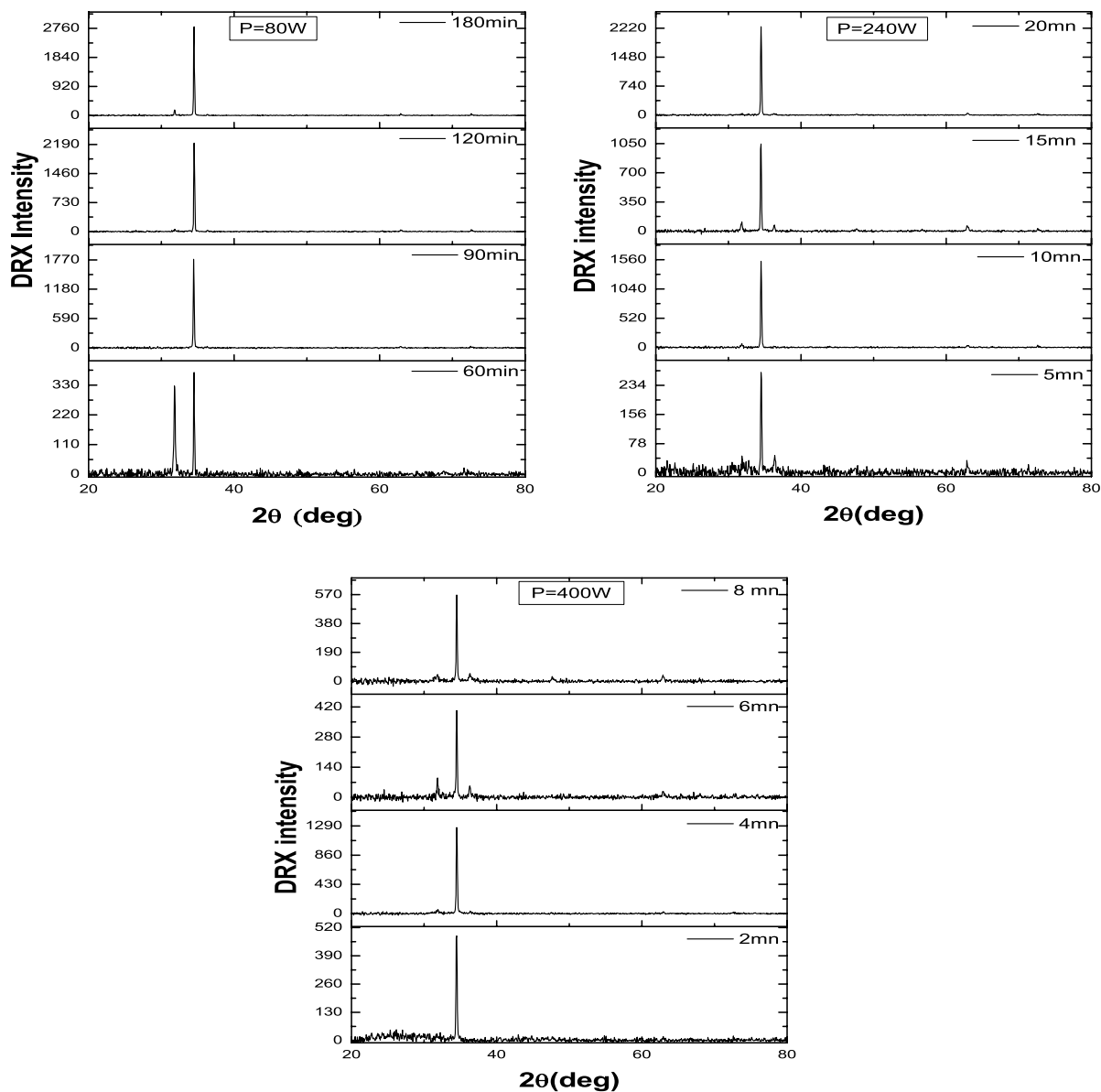


Fig. 2 XRD spectra of ZnO nanowires elaborated at different powers and deposition times

half-height width (FWHM) confirming the good crystallinity of ZnO nanowires.

The structural parameters a and c of the obtained nanowires are calculated using Bragg’s law [36] and are compared with the results reported in the literature [37].

$$2d_{hkl} \sin(\theta_{hkl}) = n\lambda \tag{1}$$

The deformation ϵ and the strain σ induced in ZnO nanowires are calculated using the following expressions [38]:

$$\epsilon = (C - C_{\text{bulk}}) / C_{\text{bulk}} \tag{2}$$

$$\sigma = \epsilon [2C_{13}^2 - (C_{11} + C_{12})C_{33}] / C_{33} \tag{3}$$

where C is the structural parameter of the nanowires, C_{bulk} the structural parameter of the bulk ZnO and C_{ij} coefficients are the elastic constants of ZnO given by the following values [39]:

$$\begin{aligned} C_{11} &= 209,7 \text{ GPa}, C_{12} = 121,1 \text{ GPa}, \\ C_{13} &= 105,1 \text{ GPa}, C_{33} = 210,9 \text{ GPa} \end{aligned} \tag{4}$$

Table 1 reports the values of the structural parameters a , c , ϵ and σ of ZnO nanowires obtained for the three series:

The calculated structural parameters show comparable values to those reported in the ZnO JCPDS 36–1451 sheet.

Table 1 Structural parameters and strains of nanowires at different powers and deposition times

Power (Watt)	Time (mins)	<i>a</i> (Å)	<i>c</i> (Å)	<i>ε</i> (%)	<i>σ</i> (GPa)
80	60	3.2435	5.1956	- 0.21	0.9507
	90	3.2327	5.2015	- 0.09	0.0440
	120	3.2401	5.1917	- 0.29	1.2877
	180	3.2432	5.1957	- 0.21	0.9420
240	5	3.2410	5.1911	- 0.30	1.3396
	10	3.2443	5.1930	- 0.26	1.1754
	15	3.2448	5.1978	- 0.17	0.7605
	20	3.2358	5.1937	- 0.25	1.1149
400	2	3.2577	5.1988	- 0.15	0.6741
	4	3.2402	5.1933	- 0.25	1.1495
	6	3.2420	5.1948	- 0.22	1.0198
	8	3.2530	5.1949	- 0.22	1.0112

Table 2 Texture coefficients of diffraction peaks for different powers and deposition times

Time (mins)	<i>T_c</i> (100)	<i>T_c</i> (002)	<i>T_c</i> (101)	<i>T_c</i> (103)
60	0.884	1.258	0.114	0.226
90	0	2.644	0.042	0.140
120	0.170	2.827	0.062	0.138
180	0.237	3.226	0.051	0.162
5	0.785	2.359	0.347	0.684
10	0.063	1.949	0	0.132
15	0.394	2.775	0.149	0.384
20	0.158	3.460	0.061	0.198
2	0	2.206	0	0.351
4	0.243	2.759	0.068	0.195
6	0.556	1.816	0.203	0.379
8	0.450	3.057	0.239	0.569

We can notice that the less constrained nanowires are those developed at 80 watts and a strong orientation along the *c* axis is obtained for a time of 90 mins confirming that the (002) surface has the lowest surface energy compared to the other surfaces of ZnO. We also note that for a power of 240 watts and 400 watts, the developed nanowires are more constrained due to random growth of nanowires in both [002] and [100] directions (Table 1).

Table 3 (002) orientation coefficient of nanowires developed for different powers and times

	Time (mins)	<i>η</i>		Time (mins)	<i>η</i>		Time (mins)	<i>η</i>
<i>P</i> = 80 W	60	1.1	<i>P</i> = 240 W	5	0.699	<i>P</i> = 400 W	2	0.853
	90	1.121		10	0.903		4	1.069
	120	1.198		15	1.118		6	0.921
	180	1.245		20	1.280		8	1.038

To quantify the degree of preferential orientation (002), the texture coefficient *T_C*(*hkl*) for each diffraction peak was calculated based on the following expression [40, 41]:

$$T_c(hkl) = \left[I(hkl)/I_0(hkl)/(1/n) \sum I(hkl)/I_0(hkl) \right] \quad (5)$$

where *T_C*(*hkl*) is the texture coefficient, *I* (*hkl*) is the intensity of the (*hkl*) plane and *n* is the order of diffraction.

The *T_C*(*hkl*) coefficients are shown in the Table 2 above for different powers and deposition times.

By carefully examining the values of the texture coefficient of the different planes (*hkl*), we can see that most of the samples show a preferential growth direction (002) corresponding to the hexagonal wurtzite phase.

The degree of preferential orientation of nanowires is given by the following relation [42]:

$$\eta = \sqrt{(T_c - 1)^2/N} \quad (6)$$

where *T_c* is the texture coefficient and *N* is the number of considered peaks.

The values *η* are grouped in Table 3. According to the orientation coefficient values, we notice that the nanowires developed at *P* = 80 watts are the most oriented (002) indicating that the kinetics of formation of well-oriented nanowires must take place under soft chemical reaction conditions.

3.2 Morphological analysis

The SEM images of developed nanowires are shown in Fig. 3. The SEM images show that ZnO nanowires are well oriented for a power *P* = 80watts and become denser and take various orientations by increasing the furnace power. This result strongly supports the results of the XRD analysis discussed above. In high powers, as shown in Fig. 3k, it is noticeable that ZnO nanowires have pyramid-shaped ends due to a decrease in OH⁻ hydroxide concentration because of the evaporation of water from the deposition solution which promotes growth in both longitudinal and lateral directions. Taking into account that longitudinal growth is faster than lateral growth, this will generate the formation of pyramidal structures.

It is to notice that the analysis of chemical composition carried out by Energy Dispersive Analysis of X-ray

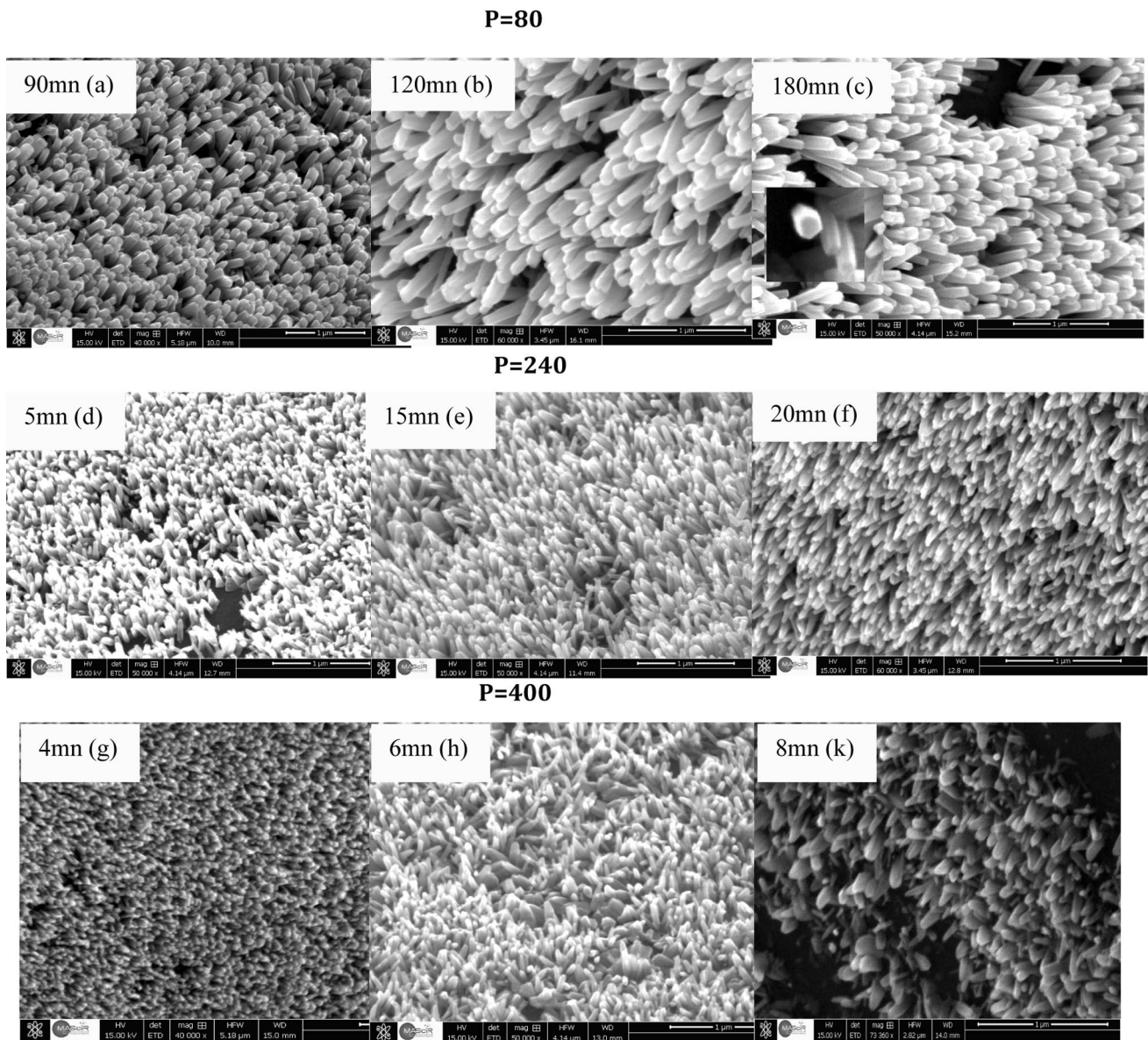


Fig. 3 SEM images of nanowires developed at different powers and deposition times

(EDAX) measurements at room temperature confirms the existence of oxygen and zinc elements in non-stoichiometric proportions (oxygen atomic content less than zinc one) leading to n-type semiconductors of obtained ZnO nanowires.

We were able to estimate by SEM the lengths and diameters of the nanowires analyzed, which we have illustrated in Table 4 below. By examining the values of the table, we can see that the length of the nanowire increases as the growing time increases and reduces with power. While for the diameter of nanowires, it varies very little for a fixed power and falls as the power rises. These results show that the length and diameter of ZnO nanowires can be controlled

by adjusting the microwave power and hence the temperature of the deposition solution as well as the deposition time.

We have represented in Fig. 4, the length of the nanowires produced at 80, 240 and 400 watts as a function of the deposition time. As demonstrated, operating at high power levels can optimize the deposition time of nanowires. Indeed, it will be possible to obtain the same length of nanowires, without losing the structural quality, by carrying out a rapid heat treatment by microwave. Hence the usefulness of the microwave furnace compared to the hydrothermal technique using the autoclave system, which requires a longer time to grow nanowires.

Table 4 Lengths and diameters of ZnO nanowires at different powers and deposition times

Power(Watt)	Growth time (mins)	Length (nm)	Diameter (nm)
80	60	236.12	94.18
	90	280.16	102.72
	120	390.47	109.14
	180	570.33	128.40
240	5	182.20	47.37
	10	218.85	56.80
	15	284.12	63.50
	20	330.51	74.01
400	2	125.83	42.43
	4	144.29	46.00
	6	184.33	50.18
	8	235.71	56.28

3.3 Optical properties

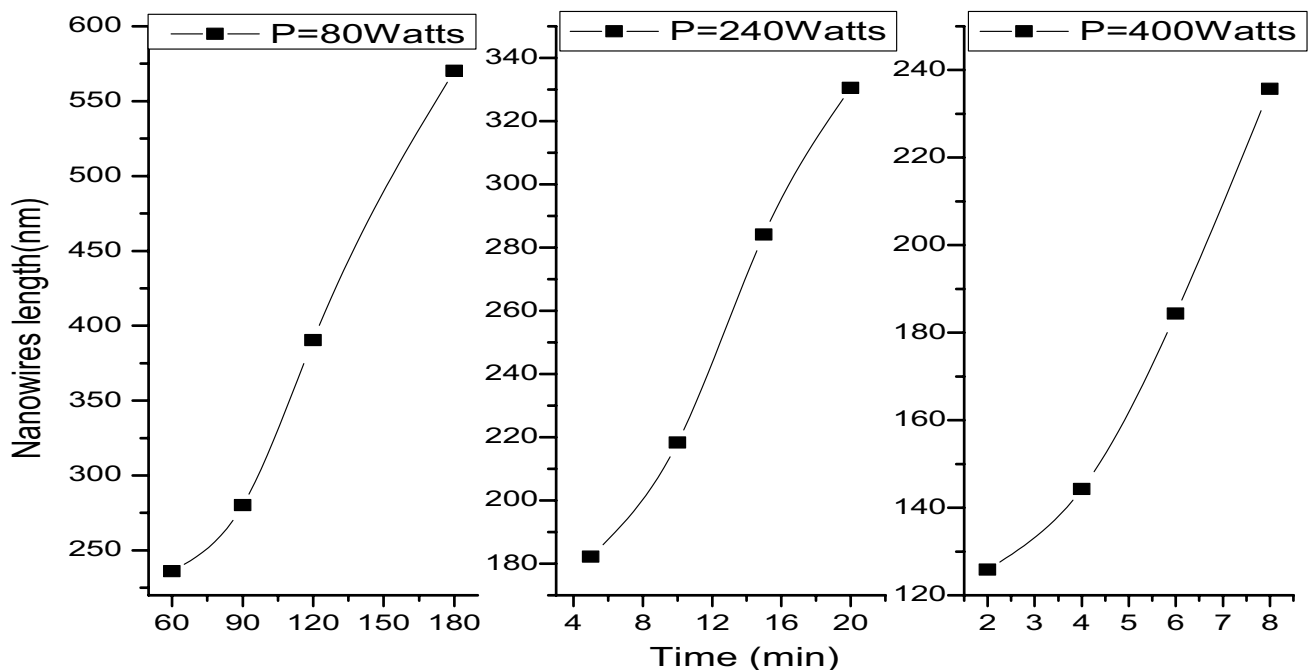
Figures 5a, b, and c illustrate the optical transmittance spectra of the nanowires of the three sample series, as a function of wavelength in the range of 200–900 nm. By analyzing these curves, we can see that all samples show a good transmittance in the near UV and visible regions with an average transmittance level of about 90%. As growth time increases, the level of transmittance in the visible region decreases regularly and appreciably for nanowires made at 80 watts.

This effect is due to the absorption of these nanowires in this domain as shown by their absorption spectra inside Fig. 5a. For the given power, we notice a narrowing of the optical window with the deposition time. We can, therefore, affirm the modulation of the gap energy of nanowires by simply varying their growth time and hence their use as an optical window in solar cells. It should also be noted that the transmittance curves have a shoulder between 300 and 350 nm that we can associate with the phase of the ZnO buffer layer where the nanowires are not developed.

In the inset of Fig. 5a, b and c, we present the absorption coefficient α for the elaborated ZnO nanowires. As shown, the samples exhibit a sharp absorption edge in the UV region in the range of 300–400 nm, which decrease with deposition time for a given power. Beyond 400 nm, the absorption coefficient tends to zero and there is no absorption in the nanowires.

The absorption threshold in the visible range is determined by the optical gap energy E_g . The Tauc plot widely used in the literature to get the bandgap is not a proper way for a crystalline material because it assumes the absorption profile following the density of states of free electrons, which is obviously incorrect due to the excitonic effect of ZnO (60 meV). Alternatively, we adopted the first derivative of the absorbance method with respect to photon energy to extract the bandgap from absorption spectra by finding the maxima in derivative spectra at lower energy sides.

The first peaks of derivative absorbance for different microwave power at different times are presented in Fig. 6.

**Fig. 4** Axial growth rate of samples at different powers and deposition times

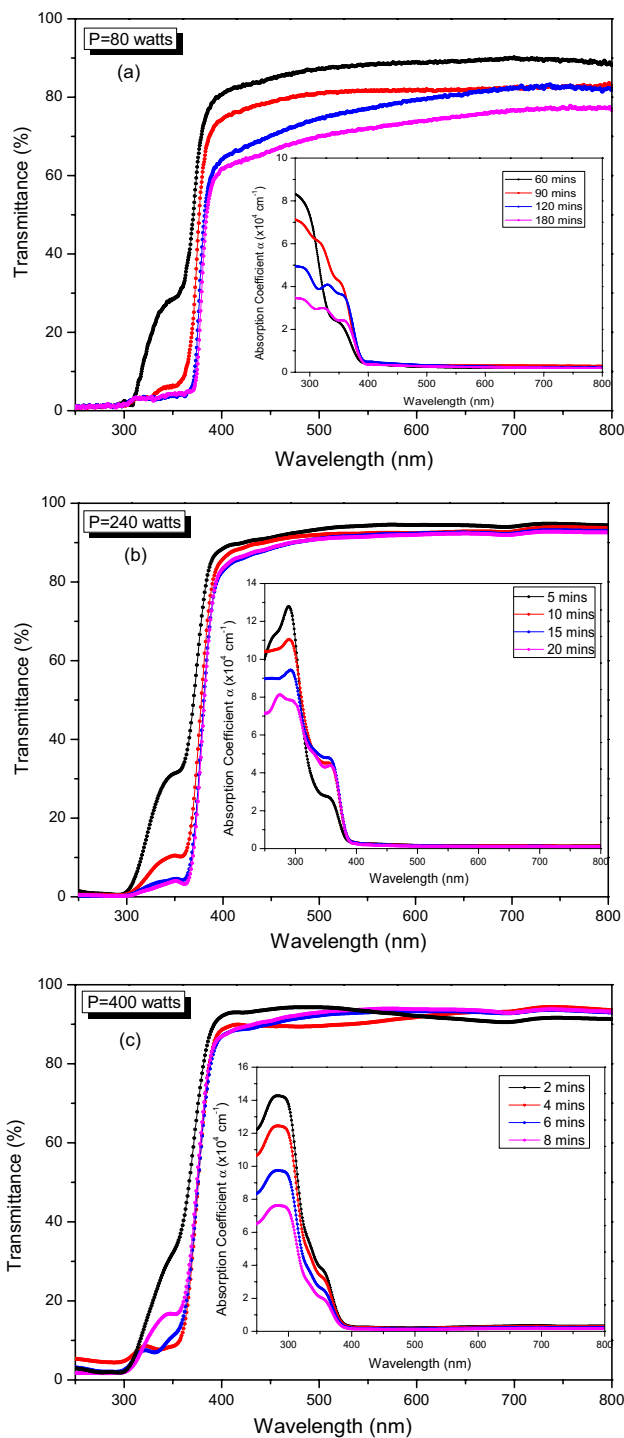


Fig. 5 Transmittance and absorption spectra of ZnO nanowires developed at different powers and deposition times

With increasing deposition time, a red shift of the absorption edge can be observed with a more pronounced shift for power $P=80$ watts, indicating a shrinking of the optical window of nanowires. This tendency of extracted gap energy versus time is shown inset the figures.

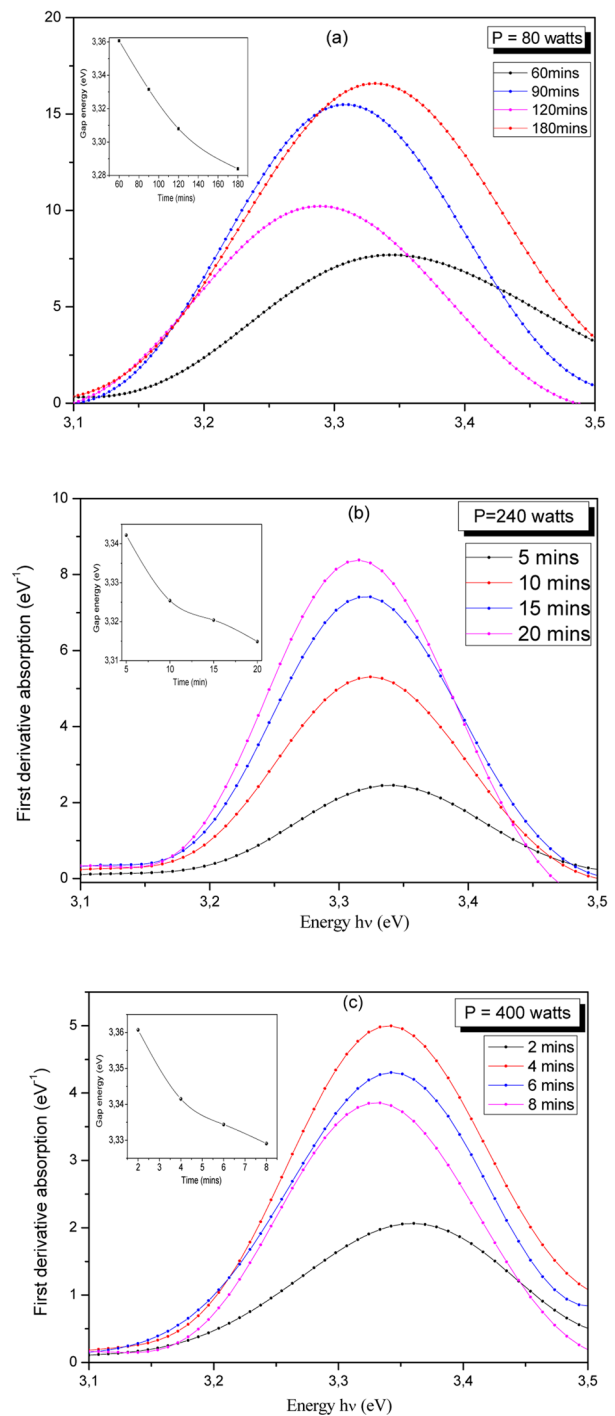


Fig. 6 First absorbance derivative versus energy at different powers and deposition times. Inset figures the plots of gap energy versus time

Table 5 reports the extracted gap energies of our samples and shows that, for a given power, the optical gap E_g decreases with the growth time (inset Fig. 6a, b, c). This result is in good agreement with the diameter data estimated above which show a correlation between the structural and electronic aspects of the developed nanowires.

Table 5 Gap energy and Urbach energy of nanowires developed at different powers and deposition times

$P=80$ Watts	Time (mins)	60	90	120	180
	E_g (eV)	3.360	3.331	3.308	3.284
	E_u (meV)	137.4	105.7	111.8	135.5
$P=240$ Watts	Time (mins)	5	10	15	20
	E_g (eV)	3.342	3.325	3.320	3.315
	E_u (meV)	91	67	79	77
$P=400$ Watts	Time (mins)	2	4	6	8
	E_g (eV)	3.360	3.341	3.334	3.329
	E_u (meV)	96.8	70.5	69.6	68.4

The n-type of our samples leads to located states at the tail of the conduction band represented by the commonly named Urbach energy E_u . This energy is determined by the relation involving the absorption coefficient α near which, the band edge shows an exponential dependence on photon energy for many materials and given by (Urbach F., 1953) [43]:

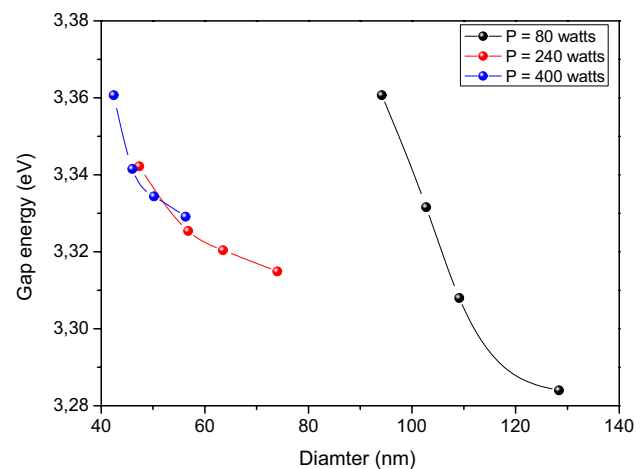
$$\alpha = \alpha_0 \exp(h\nu/E_u) \quad (7)$$

where α_0 is the pre-exponential factor. The Urbach energy E_u is obtained from the inverse of the slope acquired by fitting the linear part of $\ln\alpha$ versus $h\nu$. The E_u energy is listed in Table 5 with gap energy. The calculated Urbach energies of our samples show low values of the order of about tens meV meaning a low disorder with high crystallinity of nanowires which is in perfect agreement with XRD spectra.

To illustrate this effect, we have presented in Fig. 7, the gap energy as a function of nanowires diameter for different powers. The figure shows that the gap energy varies inversely with the diameter of the elaborated nanowires. Schneider and al [44], were among the first to study the variation of PL emission energy as well as the gap energy from InAs/InP quantum well samples as a function of well thickness with nominal well thickness ranging from 1 to 4 monolayers. The measured energies are in very good agreement with those calculated using a simple model of square wells based on the approximation of the envelope function for valence band and are decrease with the well thickness. Hence, we can then explain the bandgap change to be likely due to the elaboration conditions and to the structure changes of nanowires which can inhibit an early stage of confinement effect of the electrons along the c axis.

4 Conclusion

In this work, we have been interested in the synthesis of ZnO nanowires by a hydrothermal technique using a variable power microwave oven. The results showed that the

**Fig. 7** Variation of gap energy as a function of the calculated diameters

developed nanowires are well oriented (002) according to the hexagonal phase wurtzite. Besides, the nanowires are characterized by an increasing density and length and a decreasing diameter as the deposition time and the power of the microwave increase. It must also be noted that the obtained nanowires have an optical transmittance in the visible region of about 90% and that their gap decreases as the deposition time increases. A correlation between the diameter of the nanowires and their gap energy has been shown and confirms well that density, length, diameter, and gap energy of ZnO nanowires can be modulated by simple control of power microwave and deposition time.

Compliance with ethical standards

Conflict of interest The authors declare that they have no conflicts of interest.

References

1. X.K. Wu, W.Q. Huang, Z.M. Huang, Y.L. Tang, *Phys. E: Low-Dimens. Syst. Nanostruct.* **90**, 24–27 (2017)
2. Kavita, D. Kumar, K. Singh, S. Kumar, H.S. Bhatti, *Phys. E: Low-Dimens. Syst. Nanostruct.* **79**, 188–197 (2016)
3. P. Pascariu, C. Cojocaru, P. Samoila, A. Airinei, M. Sucheja, *J. Alloy. Compd.* **8345**, 155144 (2020)
4. Z. Huang, Y. Yan, C. Xing, Q. Wang, Y. Jiang, *J. Alloy. Compd.* **78915**, 841–851 (2019)
5. E.S. Nour, O. Nur, M. Willander, *J. Semicond. Sci. Technol.* **32**, 064005 (2017)
6. V. Srikant, D.R. Clarke, *J. Appl. Phys.* **83**(10), 5447–5451 (1998)
7. D. Chen, S. Chen, S. Yue, Lu Bin, Z. Ye, *J. Lumin.* **216**, 116719 (2019)
8. C.-Y. Chou, S.-F. Tseng, T.-L. Chang, Tu Chen-Ting, H.-C. Han, *Appl. Surf. Sci.* **5081**, 145204 (2020)
9. C. Florica, E. Matei, A. Costas, M.E.T. Molares, I. Enculescu, *Electrochim. Acta* **13710**, 290–297 (2014)
10. S.W. Kang, P.R. Deshmukh, Y. Sohn, W.G. Shin, *Mater. Today Commun.* **21**, 100675 (2019). <https://doi.org/10.1016/j.mtcom.2019.100675>
11. J. Sultana, S. Paul, R. Saha, S. Sikdar, A. Karmakar, S. Chattopadhyay, *Thin Solid Films* **699**, 137861 (2020). <https://doi.org/10.1016/j.tsf.2020.137861>
12. L. Kang, H.L. An, J.Y. Park, M.H. Hong, C.G. Lee, *Appl. Surf. Sci.* **4751**, 969–973 (2019)
13. M.H. Huang, Y. Wu, H. Feick, N. Tran, E. Weber, P. Yang, *Adv. Mater.* **13**, 113 (2001)
14. Y.C. Kong, D.P. Yu, B. Zhang, W. Fang, S.Q. Feng, *Appl. Phys. Lett.* **78**, 407 (2001)
15. J.-J. Wu, S.-C. Liu, *Adv. Mater.* **14**, 215 (2002)
16. J.-J. Wu, S.-C. Liu, *J. Phys. Chem. B* **106**, 9546 (2002)
17. H. Yuan, Y. Zhang, *J. Cryst. Growth* **263**, 119 (2004)
18. Z. Ye, J. Huang, W. Xu, J. Zhou, Z. Wang, *Solid State Commun.* **141**, 464 (2007)
19. J. Zhang, L. Sun, H. Pan, C. Liao, C. Yan, *New J. Chem.* **26**, 33 (2002)
20. Q. Li, M. An, D. Li, *Results Phys.* **12**, 1446–1449 (2019)
21. X. Chen, Y. Shen, W. Zhang, J. Zhang, Y. Shen, *Appl. Surf. Sci.* **43530**, 1096–1104 (2018)
22. P. Obreja, D. Cristea, A. Dinescu, C. Romanitan, *Appl. Surf. Sci.* **4631**, 1117–1123 (2019)
23. M. Huang, J. Cao, X. Meng, Y. Liu, L. Sun, *Chem. Phys. Lett.* **6621**, 42–46 (2016)
24. S. Tuscharoen, N. Kulakeatmongkol, M. Horprathum, K. Aiampanakit, J. Kaewkhao, *Mater. Today* **5**, 15213–15217 (2018)
25. Ji Haining, L. Dongqing, C. Haifeng, Z. Chaoyang, Z. Wenwei, *Rare Metal Mater. Eng.* **46**(12), 3601–3605 (2017)
26. E. Muchuwani, T.S. Sathiaraj, H. Nyakoty, *J. Alloy. Compd.* **72115**, 45–54 (2017)
27. M. Ayala-Torres, C. Mejía-García, E. Díaz-Valdés, J. Romero-Labias, M.G. De La Cruz-Vicencio, *Mexican society of science and technology of surfaces and materials. Surf. Vac.* **27**(1), 7–10 (2014)
28. H.E. Unalan, P. Hiralal, N. Rupesinghe, S. Dalal, W.I. Milne, G.A. Amaratunga, *Nanotechnology* **19**(25), 255608 (2008)
29. M. Guo, P. Diao, S. Cai, *J. Solid State Chem.* **178**, 1864–1873 (2005)
30. Q. Ahsanulhaq, A. Umar, Y.B. Hahn, *Nanotechnology* **18**, 115603–115610 (2007)
31. B. Postels, H.H. Wehmann, A. Bakin, M. Kreye, D. Fuhrmann, J. Blaesing, A. Hangleiter, A. Krost, A. Waag, *Nanotechnology* **18**, 195602–195609 (2007)
32. G. El Hallani, N. Fazouan, A. Liba, L. Laanab, in *Proceedings of the 2nd Edition of International Renewable and Sustainable Energy Conference (IRSEC'14)*, 82–84 (2014)
33. P.K. Samanta, S.K. Patra, P.R. Chaudhuri, *Phys. E* **41**, 664 (2009)
34. B. Weintraub, Z. Zhou, Y. Li, Y. Deng, *Nanoscale* **2**(9), 1573–1587 (2010)
35. C.M. Shin, J.H. Heo, J.H. Park, T.M. Lee, H. Ryu, B.C. Shin, W.J. Lee, H.K. Kim, *Phys. E* **43**, 54–57 (2010)
36. J. Xiaomhg, *Chinese Phys. Lett.* **8**, 356 (1991)
37. G. El Hallani, S. Nasih, N. Fazouan, A. Liba, M. Khuili, M. Sajieddine, M. Mabrouki, L. Laanab, E.H. Atmani, *J. Appl. Phys.* **121**, 135103 (2017)
38. M. Subramanian, M. Tanemura, T. Hihara, V. Ganesan, T. Soga, T. Jimbo, *Chem. Phys. Lett.* **487**, 97–100 (2010)
39. T.B. Bateman, *J. Appl. Phys.* **33**, 3309 (1962)
40. S.S. Shinde, P.S. Patil, R.S. Gaikwad, R.S. Mane, B.N. Pawar, K.Y. Rajpure, *J. Alloys Compd.* **503**, 416 (2010)
41. S.S. Shinde, P.S. Shinde, S.M. Pawar, A.V. Moholkar, C.H. Bho-sale, K.Y. Rajpure, *Solid State Sci.* **10**, 1209 (2008)
42. J. Elias, *Editions Universitaires Europeennes*, 30 avril (2010), ISBN-13: 978-6131503221
43. F. Urbach, *Phys. Rev* **92**, 1324 (1953)
44. R.P. Schneider, B.W. Wessels, *J. Electron. Mater.* **20**, 1117–1123 (1991)

Publisher's Note Springer Nature remains neutral with regard to jurisdictional claims in published maps and institutional affiliations.